Theory of the broadening of vibrational spectra induced by lowered symmetry in yttria nanostructures

H. Bao,[1] X. L. Ruan,[1,2,*] and M. Kaviany[3]
[1]*School of Mechanical Engineering, Purdue University, West Lafayette, Indiana 47907, USA*
[2]*Birck Nanotechnology Center, Purdue University, West Lafayette, Indiana 47907, USA*
[3]*Department of Mechanical Engineering, University of Michigan, Ann Arbor, Michigan 48109, USA*
(Received 16 May 2008; revised manuscript received 12 August 2008; published 23 September 2008)

We calculate the vibrational spectra for typical nanostructures including thin films, nanowires, and quantum dots of yttria, an important laser host material. Lattice dynamics calculations show that the vibrational spectra of nanocrystals are distinct from that of the bulk phase in the enhanced tails at low and high frequencies. Some of the low-frequency and high-frequency modes only involve surface atoms. Molecular-dynamics simulations are used to further decompose the contributions of surface and internal atoms, and the results confirm the evident broadening of the surface spectra. The broadening in vibrational spectra is attributed to the broadened atomic spring constants, further to the lowered symmetry of nanostructures.

DOI: 10.1103/PhysRevB.78.125417 PACS number(s): 63.22.Dc, 63.22.Gh, 63.22.Kn

I. INTRODUCTION

Vibrational properties of materials are critical in many energy conversion applications such as lasers and photovoltaics, for which efficiencies are largely dependent on electron-phonon coupling. Recently, nanocrystals have been widely used in these applications because of their favorable size effects in electronic and optical properties.[1–4] In these applications, however, the phonon spectra of nanostructures are often assumed to be the same as those of bulk phase for simplicity or due to the lack of available data. Although this approximation can be acceptable for some materials or under certain conditions, it is questionable in general. For a rigorous description of the vibrational properties and the electron-phonon coupling behavior, a thorough understanding of the size effects on phonon spectra is necessary.

There have been a considerable amount of studies on vibrational spectra of nanocrystals, which have addressed the features of spectra and their origins. A Green's function study of the vibrational spectra of metallic nanocrystals with diameters of 2–5 nm showed enhanced low-frequency and high-frequency tails, and a linear scaling of the vibrational projected density of states (DOS).[5] The low-frequency tail was proposed to be the contribution from surface atoms, which was later confirmed by a molecular-dynamics simulation where the contributions of surface and interior atoms were decomposed.[6] The high-frequency tails were also studied by molecular dynamics[7] and phonon Green's function recursion techniques,[8] and were traced to a global inward shrinking. These studies have provided excellent insights into the origins of the low-frequency and high-frequency tails but a fundamental mechanism is still to be proposed to link the vibrational spectra and the atomic structure.

In this work, we systematically analyze the vibrational spectra of representative nanostructures, including thin films, nanowires, and quantum dots (QDs). An important laser host material, Y_2O_3, is used as the model material. Lattice dynamics is first applied to calculate the normal vibrational modes and eigenvectors, allowing for a direct examination of the origin of each mode. Molecular dynamics is then employed to decompose the vibrational spectra to surface and inner regions in order to resolve their respective contributions. The force constants of surface and inner atoms are then calculated and compared to those of the bulk phase, and the relationship between the broadened vibrational spectra and the loss of translational symmetry is proposed.

II. CRYSTAL STRUCTURE AND INTERATOMIC POTENTIALS

Both lattice dynamics and molecular-dynamics calculations require a crystal structure and a set of interatomic potentials. Yttria bulk structure and three representative low-dimensional structures (thin film, nanowire, and quantum dot) are considered in this study, as shown in Fig. 1. The x-ray diffraction[9] and neutron-diffraction[10] experiments have shown that Y_2O_3 has a face-centered-cubic structure with a lattice constant of 10.604 Å and 80 atoms in a conventional unit cell. Eight yttrium ions are in the sites (1/4,1/4,1/4), and the remaining twenty–four occupy the sites $(u,0,1/4)$. The 48 oxygen ions are in general positions (x,y,z), arranged in distorted octahedra around the yttrium ions, and the yttrium-oxygen bonding distances are unequal. The values of u,x,y,z are given in Refs. 9 and 10. This lattice structure is still retained in nanocrystals[11] so we generate the low-

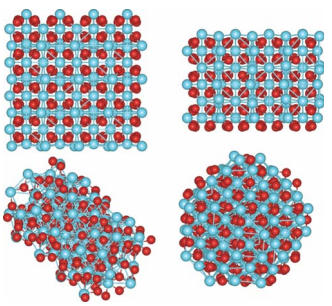

FIG. 1. (Color online) Bulk, thin film, nanowire, and quantum dot of Y_2O_3.

TABLE I. Parameters used in the Buckingham potential atomic charges: $q_Y=3$ and $q_O=-2$.

Atom-Atom	A_{ij} (eV)	$r_{0,ij}$ (Å)	C_{ij} (eV Å)	References
Y-Y	0	1	0	15
Y-O	1345.6	0.3491	0	14 and 15
O-O	22799	0.149	27.93	14 and 15

dimensional structures by cutting them out of a large bulk crystal. The surfaces are simply left with dangling bonds. The obtained raw structures are obviously not in their equilibrium configurations so they need to be relaxed through a structure optimization process.

Interatomic potentials can be obtained from experiments and/or *ab initio* calculations.[12] For yttria the many-body (>2) interactions can be neglected, left only with the self energies of single atoms and two-body interactions between atomic pairs. The two-body potentials can be assumed to be in the form

$$\varphi(r_{ij}) = \frac{q_i q_j}{r_{ij}} + A_{ij} \exp\left(-\frac{r_{ij}}{r_{0,ij}}\right) - \frac{C_{ij}}{r_{ij}^6}, \tag{1}$$

where $\varphi(r_{ij})$ is the interaction energy of atoms i and j, which consists of a Coulomb term and a covalent (short-range) contribution cast into the usual Buckingham form.[13] Here q_i is an effective charge of the ith atom, r_{ij} is the interatomic distance between atoms i and j, and A_{ij}, $r_{0,ij}$, and C_{ij} are parameters for covalent interactions. For ionic materials, this Buckingham interatomic potential model has been shown to perform well. The parameters in Eq. (1) are adopted from Refs. 14 and 15, and listed in Table I. This potential set has been verified to reproduce the bulk properties (lattice constant, lattice position, bulk modulus, elastic constant, etc.) well.[16]

III. LATTICE DYNAMICS CALCULATIONS

In this section, we use lattice dynamics calculations to analyze the formation of the low-frequency and high-frequency tails in the phonon spectra of nanostructures.

A. Dynamical matrix

Consider a crystal with each unit cell having n atoms, and denote the displacement of the jth atom in the lth unit cell by $\mathbf{u}(jl)$. We can define the lattice energy, W, as a sum over all atom-atom interactions:

$$W = \frac{1}{2} \sum_{jj',ll'} \varphi\begin{pmatrix} jj' \\ ll' \end{pmatrix}, \tag{2}$$

where $\varphi\left(\begin{smallmatrix} jj' \\ ll' \end{smallmatrix}\right)$ is the interaction energy between pair of atoms (jl) and $(j'l')$. The elements of the $3N\times 3N$ force-constant matrix (N is the total number of atoms in the system) are defined as

$$\Phi_{\alpha\beta}\begin{pmatrix} jj' \\ ll' \end{pmatrix} = \frac{\partial^2 W}{\partial u_\alpha(jl)\, \partial u_\beta(j'l')}, \tag{3}$$

where the subscripts α and β denote the Cartesian vector components x, y, and z. Then the dynamical matrix $D(\mathbf{k})$ is given by[17]

$$D_{\alpha,\beta}(jj',\mathbf{k}) = \frac{1}{(m_j m_{j'})^{1/2}} \sum_{l'} \Phi_{\alpha,\beta}\begin{pmatrix} jj' \\ ll' \end{pmatrix} \times \exp\{i\mathbf{k}\cdot[\mathbf{r}(j'l') - \mathbf{r}(jl)]\}, \tag{4}$$

where m_j is the mass of the jth atom and $\mathbf{r}(jl)$ is the position of the jth atom in the lth unit cell. In the theory of lattice dynamics, the square roots of the dynamical matrix eigenvalues are the eigenmodes, or equally, vibrational frequencies. Phonon dispersion curves are obtained by plotting the normal-mode frequencies as a function of the wave number in different directions. If the wave vectors and eigenfrequencies are known, the vibrational density of states can be computed by an integral over the first Brillouin zone. For quantum dot, which does not have the reciprocal lattice, vibrational modes can be computed to yield the vibrational spectra directly.

General utility lattice program (GULP) (Ref. 18) is employed for these calculations. Since lattice dynamics for low-dimensional systems is implemented in GULP, we treat the film, nanowire, and quantum dot as two-dimensional (2D), one-dimensional (1D), and zero-dimensional (0D) systems, respectively, instead of the common supercell approach. One lattice constant is used in the infinite dimensions along with the periodic boundary condition. All finite dimensions, i.e., the thickness of the thin film and the diameters of the nanowire and quantum dot, are chosen to be 2 nm, and free boundary conditions are used. Cutoff for short-range forces are set to be 10 Å for interaction between yttrium and oxygen, and 12 Å for interaction between oxygen atoms. Electrostatic forces are calculated by the Wolf method.[19] The optimized geometry is achieved under the constant volume condition. The phonon-dispersion curves and the vibrational density of states are then obtained.

B. Vibrational density of states and dispersion curves

The normalized vibrational density of states of the bulk, thin film, nanowire, and quantum dot are shown in Fig. 2. Note that for the quantum dot the Brillouin zone is simply a single point and the calculated eigenvalues are discrete; hence a broadening factor is applied to obtain the continuous-like DOS in order to compare with other structures. With the loss of periodicity, the DOS exhibits tails at low and high frequencies, similar to the effects observed for metallic nanocrystals,[5] MgO nanocrystals,[7] and silicon nanostructures.[20] Using a visualization program GDIS,[21] the vibrational pattern of each mode can be examined. We notice that some low-frequency and high-frequency modes of nanostructures only involve surface atoms. Two such normal modes of the thin film are shown in Fig. 3 with wave vector $\mathbf{k}=0$ (Γ point), and frequencies of 34 and 866 cm^{-1}. These two modes are not present in the bulk phase of a same simu-

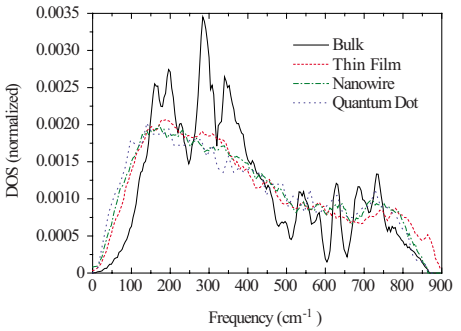

FIG. 2. (Color online) Vibrational density of states of bulk, thin film, nanowire, and quantum dot calculated by lattice dynamics.

lation size, indicating that in nanostructures new surfaces modes with high and low frequencies are promoted.

Dispersion curves are also calculated for the [001] direction for the bulk system, [01] direction for the thin film, and axial direction for nanowire, as shown in Fig. 4. Only the dispersion curves and DOS between 0 and 100 cm^{-1}, and between 800 and 900 cm^{-1} are shown for our interest in the low-frequency and high-frequency tails. Comparing to bulk, the dispersion curves for nanostructures are different in a few ways at low and high frequencies. The three acoustic branches of the film and nanowire have smaller slopes, implying a smaller sound velocity. Also the low-frequency optical branches shift toward lower frequencies. These lead to the DOS enhancement at low frequency for the thin film and nanowires. On the other hand, optical branches are flatter at high frequency near the cutoff, resulting in the DOS enhancement at the high-frequency tail.

IV. MOLECULAR-DYNAMICS SIMULATIONS AND THE VIBRATIONAL SPECTRA DECOMPOSITION

We then use molecular-dynamics simulations to further study the vibrational spectra broadening. In a molecular-dynamics simulation, the phase-space trajectory of a system of particles is predicted by solving Newton equations. The vibrational density of states is then calculated through the velocity-velocity autocorrelation function.[22] Unlike lattice dynamics, molecular-dynamics simulations are not capable of calculating the exact eigenfrequencies and eigenvectors of normal vibrational modes, but molecular dynamics can include the anharmonic effects at finite temperatures. In addition, it can simulate much larger systems than lattice dynamics since the direct diagonalization of the large scale matrix can become inefficient or even impractical.

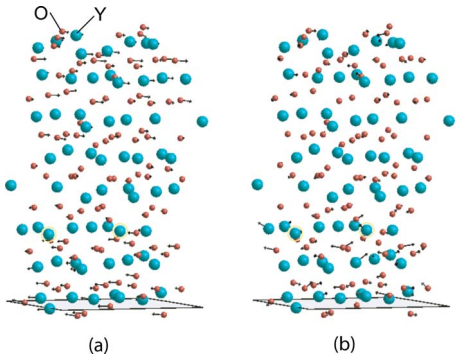

FIG. 3. (Color online) Normal modes with zero wave vector, and of frequencies of (a) 34 and (b) 866 cm^{-1}. Arrows are the maximum displacements of atoms and the parallelograms are the 2D unit cells. The vertical direction is finite.

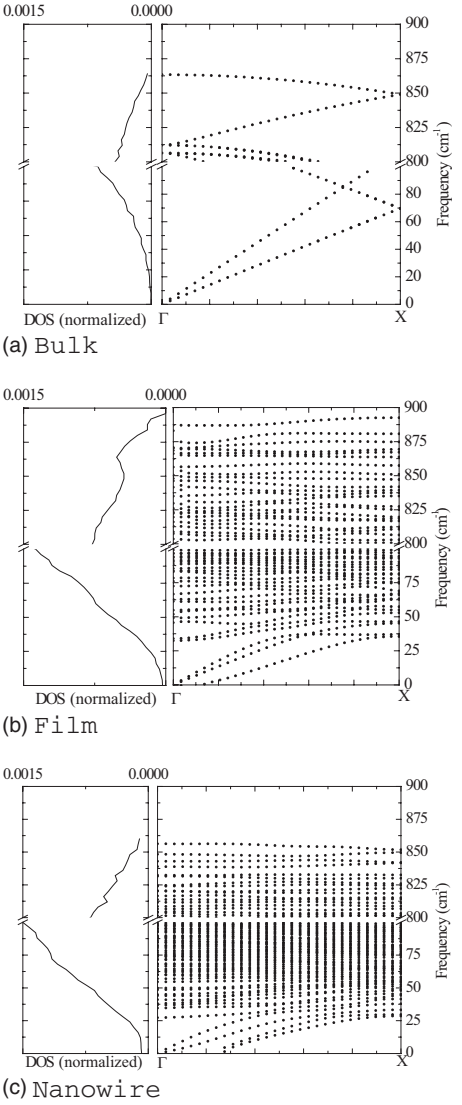

FIG. 4. Vibrational DOS and dispersion in [001] direction for bulk, [01] direction for thin film, and dispersion for nanowire structures.

A. Simulation procedure

Here, threefolds of the lattice constant are used for periodic direction(s) with the periodic boundary condition, and 5 nm is used for confined direction(s) along with the free boundary condition. The time step is chosen to be 1.6 fs. An *NVT* (constant mass, volume, and temperature) ensemble of 1×10^4 time steps is used to initialize the system to 300 K. The system is then switched to *NVE* (constant mass, volume, and energy) ensemble to run for another 4×10^4 time steps. Positions and velocities are recorded during this process.

B. Decomposition of vibrational spectra

For bulk solids, the normalized velocity-velocity autocorrelation function is usually determined for each species. Here we have yttrium and oxygen atoms, and the autocorrelation function for the species α (α=Y,O) is

$$\Gamma_\alpha(t) = \left\langle \sum_{i_\alpha=1}^{N_\alpha} \mathbf{v}_{i_\alpha}(t)\mathbf{v}_{i_\alpha}(0) \right\rangle \Bigg/ \left\langle \sum_{i_\alpha=1}^{N_\alpha} \mathbf{v}_{i_\alpha}(0)\mathbf{v}_{i_\alpha}(0) \right\rangle, \quad (5)$$

$$\alpha = \mathrm{Y,O},$$

where N_α is the number of atoms of species α, $\mathbf{v}_{i_\alpha}$ is the velocity of atom i_α, and $\langle\ \rangle$ is an ensemble average.

For nanocrystals, the internal and surface atoms have different vibrational behaviors. The crystal structure of the internal region still retains that of bulk crystals, which implies that the internal atoms will likely behave as if they were in a bulk crystal. On the other hand, the surface structure deviates significantly from the bulk phase since surface atoms lose their outer neighbors, leading to different bond lengths, bond angles, etc. Therefore, it is straightforward to us to analyze regions from the interior to surface separately. Following this path, atoms are divided into different groups according to both species and locations.[6] To make such decomposition, we define a parameter R as the distance from an atom to the center layer (for the film), center axis (for the nanowire), or sphere center (for the quantum dot). Surface atoms are those with $R>2$ nm, intermediate with 1.5 nm$>R>1$ nm, and interior with $R<0.5$ nm. The autocorrelation function for species α (α=yttrium, oxygen) at region β (β=surface, intermediate, internal) is given by

$$\Gamma_{\alpha\beta}(t) = \left\langle \sum_{i_{\alpha\beta}=1}^{N_{\alpha\beta}} \mathbf{v}_{i_{\alpha\beta}}(t)\mathbf{v}_{i_{\alpha\beta}}(0) \right\rangle \Bigg/ \left\langle \sum_{i_{\alpha\beta}=1}^{N_{\alpha\beta}} \mathbf{v}_{i_{\alpha\beta}}(0)\mathbf{v}_{i_{\alpha\beta}}(0) \right\rangle, \quad (6)$$

where the double subscript $\alpha\beta$ denotes atoms of species α and in region β, then $N_{\alpha\beta}$ is the number of atoms of species α and in region β.

The frequency spectrum of the normalized velocity autocorrelation function gives the partial vibrational DOS $D_{p,\alpha\beta}(\omega)$ as

$$D_{p,\alpha\beta}(\omega) = \int_0^\tau \Gamma_{\alpha\beta}(t)\cos\ \omega t dt, \quad (7)$$

where τ is infinity in principle, and in our calculation it is set to be a sufficiently large value such that the integral does not change. Generally, the partial vibrational density of states calculated in this way can only give the shape of the spectrum while the absolute values are meaningless. Recognizing that a system with $N_{\alpha\beta}$ atoms has $3N_{\alpha\beta}$ modes, where three is the number of degrees of freedom, we can scale $D_{p,\alpha\beta}(\omega)$,

$$D_{p,\alpha\beta,N_{\alpha\beta}} = c_1 D_{p,\alpha\beta}, \quad (8)$$

where c_1 is a constant such that

$$\int_0^\infty [D_{p,\alpha\beta,N_{\alpha\beta}}(\omega)d\omega] = 3N_{\alpha\beta}. \quad (9)$$

Then these partial vibrational DOSs are addable, and the total vibrational density of states of a system is just the summation of the partial vibrational DOS:

$$D_p(\omega) = \sum_\alpha \sum_\beta D_{p,\alpha\beta,N_{\alpha\beta}}. \quad (10)$$

To compare the spectra shape for systems with different number of atoms, it is necessary to define a normalized partial phonon density of states as

$$D^*_{p,\alpha\beta} = \frac{D_{p,\alpha\beta,N_{\alpha\beta}}}{3N_{\alpha\beta}}. \quad (11)$$

Therefore $D^*_{p,\alpha\beta}(\omega)$ satisfies the condition

$$\int_0^\infty D^*_{p,\alpha\beta}(\omega)d\omega = 1, \quad (12)$$

and therefore it is called a normalized partial phonon DOS.

These normalized partial phonon DOSs can be used as building blocks for higher level partial DOSs. For example, the normalized partial DOS for the species α is given by

$$D^*_{p,\alpha} = \sum_\beta \frac{c_{\alpha\beta}}{c_\alpha} D^*_{p,\alpha\beta}, \quad (13)$$

where c_α is the population weight for species α, given by

$$c_\alpha = \sum_\beta c_{\alpha\beta}. \quad (14)$$

Similarly, the normalized partial DOS for the region β is given by

$$D^*_{p,\beta} = \sum_\alpha \frac{c_{\alpha\beta}}{c_\beta} D^*_{p,\alpha\beta}, \quad (15)$$

where c_β is the population weight for region β, given by

$$c_\beta = \sum_\alpha c_{\alpha\beta}. \quad (16)$$

The total phonon DOS is obtained by summing over the partial DOS weighted with the population, i.e.,

$$D^*_p = \sum_\alpha \sum_\beta c_{\alpha\beta} D^*_{p,\alpha\beta}. \quad (17)$$

C. Vibrational spectra decomposition results

The velocity-velocity autocorrelation functions are calculated for the bulk, film, nanowire, and quantum dot. Then Fourier transform is applied and the vibrational DOS is acquired. Total vibrational DOS is shown in Fig. 5. The vibrational frequencies of yttrium atoms are considerably lower than those for oxygen atoms. It is reasonable because yttrium atom (atomic mass 88) is much heaver than oxygen atoms (atomic mass 16). Comparing bulk and other systems, low-frequency and high-frequency enhancement of low-dimensional structures is clear.

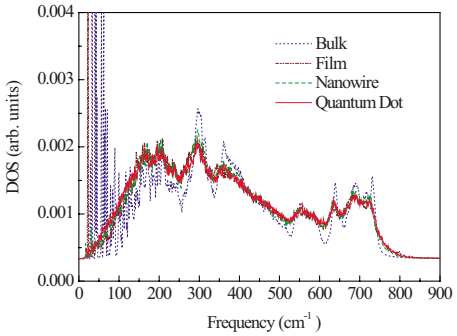

FIG. 5. (Color online) Vibrational density of states of bulk, thin film, nanowire, and quantum dot calculated by molecular dynamics.

Figure 6 shows a partial vibrational DOS of nanostructures; DOS broadening at high and low frequencies decreases from surface to interior. These results further confirm that both low-frequency and high-frequency enhancements are primarily due to surface atoms.

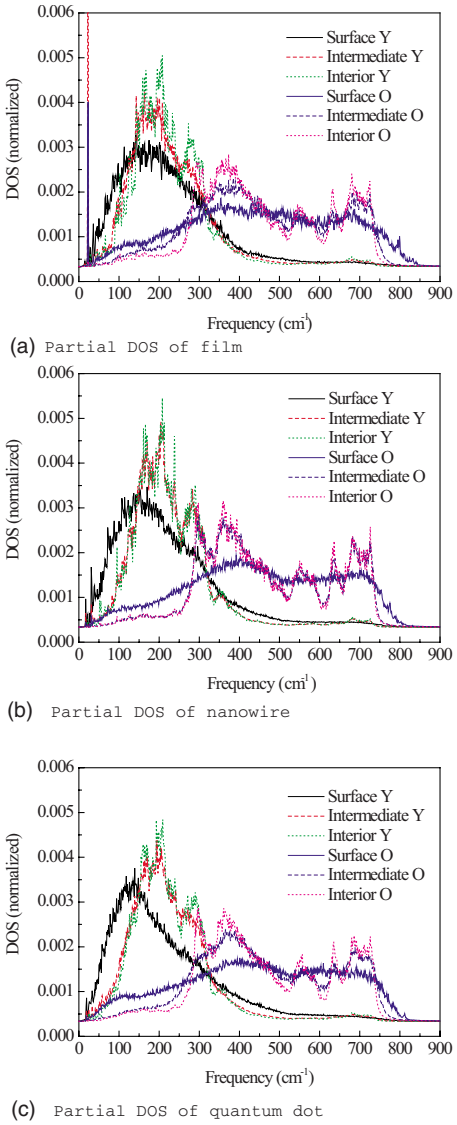

FIG. 6. (Color online) Molecular-dynamics results: partial vibrational DOS of thin film, nanowire, and quantum dot.

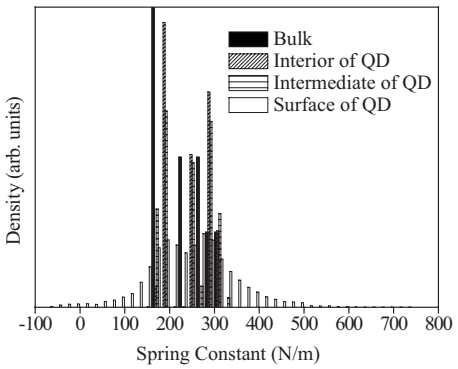

FIG. 7. Spring constant spectra for bulk and interior, intermediate, and surface atoms of QD.

V. SPRING CONSTANT BROADENING AND LOSS OF TRANSLATIONAL SYMMETRY

Two mechanisms have been proposed to explain the low-frequency and high-frequency tails, respectively:[5–8] (1) With the loss of neighbor atoms, surface atoms have lower coordinate numbers, making the surface softer and resulting in the low tail; and (2) without the "drag force" outside, all atoms tend to shrink inward, making the structure "harder" and leading to the high tail.

Here, using our decomposition approach, we can reexamine these mechanisms in a more fundamental way. Recognizing that the force constants for each atom are essential in both lattice dynamics and molecular-dynamics calculations, we calculate the distribution of atomic force constants for bulk and nanostructures. Structure optimization is performed first so that each atom is at its equilibrium position. We then displace an atom by a small value Δr and calculate the restoring force ΔF. The spring constant on this atom is calculated using $k=-\Delta F/\Delta r$. Each atom is displaced along x, y, and z directions, respectively, where the coordinate is chosen to be the lattice vectors of the conventional cell when we generate the initial structures. Calculations are done on bulk structures as well as nanostructures with a 5 nm size, and atoms in nanostructures are again decomposed into different groups based on their locations.

We calculate the spring constants for the bulk phase and quantum dot, and the values are compared in Fig. 7, where all values are placed into 45 bins covering the range from −100 to 800 N/m, with the width for each bin being 20 N/m. Due to an almost perfect spherical symmetry, the spring constant spectra do not show any difference among x, y, and z directions so we do not decompose them here. As shown, spring constants for the bulk phase are well concentrated, due to their periodicity and high symmetry. Spring constant distribution of interior atoms for quantum dots is similar to bulk, showing sharp peaks and a good concentration. This indicates that the interior atoms experience similar environment with the bulk phase. In contrast, the spring constant distribution for intermediate atoms is broadened, indicating that some atoms are in a "harder" environment while some else are in a "softer" environment. The spectrum is even more broadened for surface atoms. A few negative spring constants are present since atoms are not exactly in their

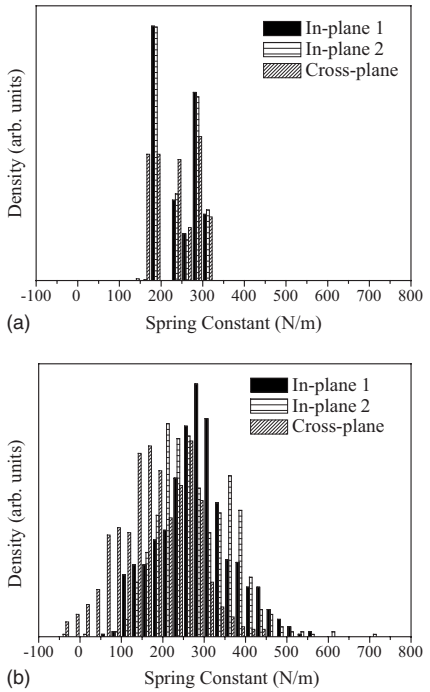

FIG. 8. Directional spring constant distribution for thin film: (a) interior and (b) surface regions.

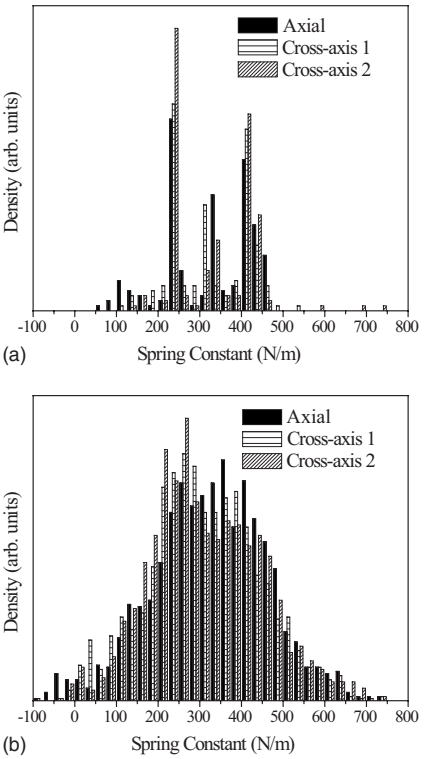

FIG. 9. Directional spring constant distribution for nanowire: (a) interior and (b) surface regions.

equilibrium positions before the displacement. Similar trends in broadening are also observed for thin films and nanowires. Note that since thin films and nanowires are anisotropic in x, y, and z directions, their broadened spectra also show some anisotropic features. For example, spring constant distributions for a thin film in the two regions and three different directions are shown in Fig. 8. For the interior region, the spring constant is similar with bulk, showing little broadening. There is no noticeable difference in the three directions, indicating an almost isotropic behavior. In contrast, spring constants for surface atoms have a much wider distribution, as expected. Also, the cross-plane spring constants have smaller values than those of the in-plane directions. Therefore, surface atoms experience a "harder" environment in the in-plane direction than the cross-plane direction. Similar trends are observed in nanowires, as shown in Fig. 9. The spring constants for the internal region show little broadening while those for the surface are evidently broadened. Also, for surface atoms, the spring constants in the cross-axis directions are only slightly smaller than those in the axial direction, indicating that anisotropic effects are reduced in lower dimensional structures.

Broadening in the spring constant spectra of surfaces implies that, in addition to the well-known softening effects, some surface atoms, however, experience the hardening environment because for these atoms the bond shrinking wins over the reduction in the coordination number. A broadened spring constant spectrum will naturally give a broadened phonon DOS. Therefore, the surfaces of nanostructures are softened at some locations and directions while some are hardened at the other locations and directions, which result in DOS enhancements at both high and low frequencies.

We notice that the translational symmetry of nanostructures is broken down from the interior to the surface. With the loss of translational symmetry, the systems no longer keep the bulk properties and a larger spread of all system properties is observed. For this reason, we can ultimately attribute the broadened spring constant spectra and vibrational spectra to the loss of translational symmetry of nanostructures from the interior to the surface.

VI. DISCUSSIONS AND CONCLUSIONS

In summary, we have calculated and analyzed the vibrational spectra of low-dimensional structures. Compared to that of the bulk phase, these spectra are broadened to result in tails at low and high frequencies. The vibrational spectra are decomposed using molecular-dynamics simulations, and the results show evident broadening in the surface spectra and moderate broadening in the interior spectra. An examination of the decomposed spring constant spectra shows that the broadened vibrational spectra can be ultimately attributed to the lowered symmetry of nanostructures, thus allowing the interpretation of both low-frequency and high-frequency tails in an integrated manner.

ACKNOWLEDGMENTS

The authors are grateful for the valuable discussions with Alan McGaughey. This work was partly supported by a faculty startup fund from Purdue University. X.L.R. also acknowledges the support by the University of Michigan, Ann Arbor. M.K. acknowledges the support through NSF Grant No. CTS-0553651.

*Author to whom correspondence should be addressed. ruan@purdue.edu

[1] D. Williams, B. Bihari, B. Tissue, and J. McHale, J. Phys. Chem. B **102**, 916 (1998).
[2] G. R. Williams, S. B. Bayram, S. C. Rand, T. Hinklin, and R. M. Laine, Phys. Rev. A **65**, 013807 (2001).
[3] X. L. Ruan and M. Kaviany, Phys. Rev. B **73**, 155422 (2006).
[4] A. Nozik, Annu. Rev. Phys. Chem. **52**, 191 (2001).
[5] A. Kara and T. S. Rahman, Phys. Rev. Lett. **81**, 1453 (1998).
[6] P. M. Derlet, R. Meyer, L. J. Lewis, U. Stuhr, and H. Van Swygenhoven, Phys. Rev. Lett. **87**, 205501 (2001).
[7] B. Wassermann and K. H. Rieder, Phys. Rev. Lett. **88**, 045501 (2002).
[8] P. M. Derlet and H. V. Swygenhoven, Phys. Rev. Lett. **92**, 035505 (2004).
[9] M. Paton and E. Maslen, Acta Crystallogr. **19**, 307 (1965).
[10] B. O'Connor and T. Valentine, Acta Crystallogr., Sect. B: Struct. Crystallogr. Cryst. Chem. **25**, 2140 (1969).
[11] A. Konrad, U. Herr, R. Tidecks, F. Kummer, and K. Samwer, J. Appl. Phys. **90**, 3516 (2001).
[12] F. Chou, J. Lukes, X. Liang, K. Takahashi, and C. Tien, Annu. Rev. Heat Transfer **10**, 141 (1999).
[13] R. Buckingham, Proc. R. Soc. London, Ser. A **168**, 234 (1938).
[14] G. Lewis and C. Catlow, J. Phys. C **18**, 1149 (1985).
[15] H. Brinkman, W. Briels, and H. Verweij, Chem. Phys. Lett. **247**, 386 (1995).
[16] M. Kilo, R. A. Jackson, and G. Borchardt, Philos. Mag. **83**, 3309 (2003).
[17] M. T. Dove, *Introduction to Lattice Dynamics* (Cambridge University Press, Cambridge, England, 1993).
[18] J. Gale, Mol. Simul. **29**, 291 (2003).
[19] D. Wolf, P. Keblinski, S. Philpot, and J. Eggebrecht, J. Chem. Phys. **110**, 8254 (1999).
[20] Z. Tang and N. R. Aluru, Phys. Rev. B **74**, 235441 (2006).
[21] http://gdis.seul.org/
[22] J. Dickey and A. Paskin, Phys. Rev. **188**, 1407 (1969).